Available online at www.sciencedirect.com
SCIENCE DIRECT®
Microelectronic Engineering 81 (2005) 544–552
MICROELECTRONIC ENGINEERING
www.elsevier.com/locate/mee

Simulation of multiple-gate quantum stub transistor

Edval J.P. Santos *, Alexandre B. Guerra

Laboratory for Devices and Nanostructures, Departamento de Eletrônica e Sistemas, Universidade Federal de Pernambuco, C.P. 7800, 50670-000, Recife-PE, Brazil

Available online 7 April 2005

Abstract

The quantum stub transistor has the potential for ultrafast, ultra low power signal processing in high density integrated circuits. However, the single gate stub transistor presents the shortcoming of requiring highly precise gate voltage to close the channel. By using a tight-binding model, we have shown that the multiple gate configuration can be used to reduce this problem. Besides, stubbed waveguides are known to develop a band structure, we propose that a stubbed wire with spin–orbit coupling (Rashba effect) could be used for spin polarized transport. This is an interesting feature, which can be used for spintronics devices. We also discuss how the Rashba effect is incorporated in our simulation program.

Keywords: Stub transistor; Simulation; Multiple gate

1. Introduction

Quantum stub transistor is based on the interference among paths as the carrier travels in the device. The electron has two main paths, one straight from source to drain and the other going by the stubs. These trajectories interfere constructively and destructively, depending on the stub length. The variation of the stub length may be accomplished by using a voltage applied to the stub. As a result, the conductance, G, as a function of the stub voltage displays an oscillatory behavior. A minimum of G is a reflection resonance or antiresonance and a maximum of G is a transmission resonance or just resonance. The transmission zeroes occur as a function of the length of the stub, L_{stub}, given by $kL_{\text{stub}} = n\pi$, and the resonances are given by $kL_{\text{stub}} = (n + 1/2)\pi$. Although, such device is conceptually simple, it presents the shortcoming of requiring highly precise gate voltage to close the channel [1–14].

Spintronics has attracted very much attention because it opens the possibility of using spin degrees of freedom to process information in advanced integrated circuits [15]. Despite its great potential, spintronics has suffered difficulties from

* Corresponding author.
E-mail address: edval@ee.ufpe.br (E.J.P. Santos).

0167-9317/$ - see front matter
doi:10.1016/j.mee.2005.03.059

the technological standpoint, because it would be necessary to use ferromagnetic materials to polarize and to analyse the spin current. Ferromagnetic materials are used to generate the magnetic field to split the electron energy levels as a result of the Zeeman effect. Such materials are not compatible with standard semiconductor processing and beyond that magnetic fields are not easy to confine. Even if the compatibility problem is solved, practical devices would require magnetic materials capable of generating strong enough fields in small volumes. One alternative is the use of the spin–orbit coupling in semiconductor crystals to achieve the required energy level splitting, this is known as the Rashba effect. The spin–orbit interaction is well known for bound electrons [16–19].

Stubbed waveguides are known to develop a band structure [21]. We propose that a multiple gate stub transistor presents less demanding voltage requirements to close the channel, and should the channel display the spin–orbit coupling, it will transport selectively spin up or spin down carriers, and therefore could be used for spin polarized transport. The simulation of double- and triple-gate stub transistor with no spin–orbit coupling is presented. This behavior can be calculated by using the recursive Green function technique as proposed by MacKinnon [22] and used to calculate the conductance of many nanodevices [22–25]. We also discuss how the Rashba effect can be incorporated in our simulation program. The paper is divided into five parts: introduction, spin–orbit coupling, simulation of electron transport, results and conclusions.

2. Spin–orbit coupling

The spin–orbit coupling term is well known for bound electrons, it can also be derived for electrons in vacuum by applying the Foldy–Wouthuysen transformation [29,30] to the Dirac equation, expanding it in v/c. Assuming $\nabla \times \mathscr{E} = 0$. $(\nabla \times (\mathscr{E}\Psi) = (\nabla\Psi) \times \mathscr{E} + (\nabla \times \mathscr{E})\Psi)$.

$$H_{SO} = -\frac{e\hbar}{4m^2c^2}\mathscr{E}\cdot\boldsymbol{\sigma}\times\boldsymbol{p} = \frac{e\hbar}{4m^2c^2}\nabla V\cdot\boldsymbol{\sigma}\times\boldsymbol{p} \rightarrow \frac{\alpha}{\hbar}[\boldsymbol{\sigma}\times\boldsymbol{p}]\cdot\hat{\boldsymbol{z}} = \frac{\alpha}{\hbar}(\sigma_x p_y - \sigma_y p_x), \quad (1)$$

where $\mathscr{E} = (0, 0, \mathscr{E}_z)$ is the electric field in the z-direction, σ are the Pauli spin matrices, $\sigma_x = |\uparrow\rangle\langle\downarrow| + |\downarrow\rangle\langle\uparrow|$, $\sigma_y = -i|\uparrow\rangle\langle\downarrow| + i|\downarrow\rangle\langle\uparrow|$, $\sigma_z = |\uparrow\rangle\langle\uparrow| - |\downarrow\rangle\langle\downarrow|$, and p is the momentum of the electron. The coupling strength, α, treated as a constant, is inversely proportional to the energy gap and the effective mass of the material used [20,26],

$$\alpha \sim \frac{e\hbar^2}{4m_0^2c^2}\frac{\mathscr{E}_z}{(m^*)^2} \sim (6\times10^{-45})\frac{\mathscr{E}_z}{(m^*)^2} J.m. \quad (2)$$

The electric field may be induced by the bulk inversion asymmetry (Dresselhaus effect) or the structure inversion asymmetry. The structure inversion asymmetry may be due to the structure of the semiconductor crystal, or the confinement potential [16]. This later effect is known as Rashba effect or Rashba mechanism, after Emmanuel I. Rashba studied it in crystals. The asymmetry of the confinement potential is of particular interest because it is not related to a particular crystal structure. The confinement potential may result from the built-in or applied potential, and therefore may be tailored by device design. The spin–orbit splitting has been observed successfully in compound semiconductors, using a gate to control the coupling [17,18]. The experimentally observed α values are 0.9×10^{-11} eV m, with carrier concentration $1.9\times10^{12}\,\mathrm{cm}^{-2}$ in InGaAs [17], and 0.6×10^{-11} eV m, with a carrier concentration of $1.0\times10^{16}\,\mathrm{cm}^{-2}$ in InAs, and does not change much with electron density. In silicon, the structure inversion asymmetry induced splitting is small [16]. The effect is also expected in 1D structures [19,20,31].

In this work, the geometry shown in Fig. 1 is considered. The carrier propagates in the y-direction, and is confined in the x- and z-directions.

To study the behavior of charge carriers, it is necessary to build a model Hamiltonian. The model Hamiltonian for the 2D wire shown in Fig. 1, is presented in Eq. (3).

$$H = \frac{p_x^2}{2m_x} + \frac{p_y^2}{2m_y} + \frac{p_z^2}{2m_z} + V(x,z) + \frac{\alpha}{\hbar}[\sigma_x p_y - \sigma_y p_x], \quad (3)$$

where $V(x,z)$ is the confining potential, and $\mathscr{E} = (0, 0, \mathscr{E}_z)$ is the electric field in the z-direction.

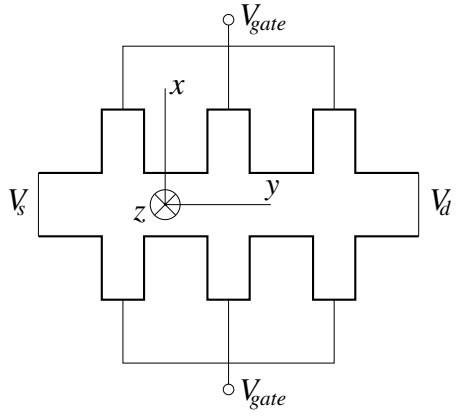

Fig. 1. Device geometry for the multiple-gate quantum stub transistor. V_s is the source voltage, V_d is the drain voltage, and V_{gate} is the gate voltage.

For this calculation, the z-dependence is not considered, except for the electric field, which is hidden into α, and $m_x = m_y = m$.

$$H = \frac{p_x^2}{2m} + \frac{p_y^2}{2m} + V(x) + \frac{\alpha}{\hbar}[\sigma_x p_y - \sigma_y p_x] = H_0 + \frac{\alpha}{\hbar}[\sigma_x p_y - \sigma_y p_x]. \quad (4)$$

In this paper, the only source of spin–orbit (SO) coupling is the field in the z-direction. The unperturbed Hamiltonian, H_0, has solutions of the form:

$$\Psi_n^{(0)}(x,y) = C_n \phi_n(x) e^{ik_y y}, \quad (5)$$

where $\phi_n(x)$ is dependent on the confining potential. To calculate $\phi_n(x)$, one needs to solve: $\frac{p_x^2}{2m}\phi_n(x) + V(x)\phi_n(x) = E_n^{(x)}\phi_n(x)$. For a infinite potential well (hard wall potential) for $|x| > b/2$, $\phi_n(x) = \sqrt{\frac{2}{b}}\cos\left(\frac{(2n-1)\pi}{b}x\right)$, and $\phi_n(x) = \sqrt{\frac{2}{b}}\sin(\frac{2n\pi}{b}x)$ for $n = 1, 2, 3, \ldots$ For a parabolic potential, $V(x) = M\omega^2 x^2/2$, $\phi_n(x) = H_n(x)$ is the Hermite polynomial of nth order.

As the coupling is considered weak, the effect of the spin–orbit coupling is taken into account through first order perturbation theory [20].

$$\begin{bmatrix} H_0 - E & \alpha\frac{d}{dx} - i\alpha\frac{d}{dy} \\ -\alpha\frac{d}{dx} - i\alpha\frac{d}{dy} & H_0 - E \end{bmatrix} \quad (6)$$

Assuming that the potential has a reflection symmetry in the x-direction, neglecting mixing between subbands, $\int \phi_m^*(x)(d/dx)\phi_n(x) = 0$ [21]. Using the unperturbed wavefunctions to calculate the matrix elements for the n-th subband, one gets:

$$\begin{bmatrix} E_n^{(0)} - E & \alpha k_y \\ \alpha k_y & E_n^{(0)} - E \end{bmatrix}, \quad (7)$$

where $E_n^{(0)}$ is the energy of the n-band of the unperturbed problem.

Solving for the eigenvalues, the energy splitting is directly proportional to the spin–orbit coupling strength. The dispersion relation is shown in Fig. 2. The coupling generates two parabolic curves, E^+ and E^-.

$$E_\pm(k_y) = E_n^{(0)} \pm \alpha k_y = E_{n_x} + \frac{\hbar^2}{2m}k_y^2 \pm \alpha k_y \quad (8)$$

The results presented so far is for a single cross-section of the device. When the slices are placed together with periodicity a, the energy levels of the slices will split, as a result of the periodicity of the structure. This result is well known in tight-binding Hamiltonians.

$$E_{n_x} \to E_{n_x} - 2t\cos(k_y a) \pm 2it_{so}\sin(k_y a) \quad (9)$$

Solving for k_y yields four solutions.

$$k_y a = \left[-\frac{t_{so}}{t} \pm \sqrt{\frac{E_F}{t}\left(\frac{E}{E_F} - \frac{E_n}{E_F}\right) + \frac{t_{so}^2}{t^2}}\right] \quad (10)$$

$$k_y a = \left[+\frac{t_{so}}{t} \pm \sqrt{\frac{E_F}{t}\left(\frac{E}{E_F} - \frac{E_n}{E_F}\right) + \frac{t_{so}^2}{t^2}}\right] \quad (11)$$

where $t = \hbar^2/2ma^2 = E_F\lambda_F^2/(2\pi a)^2$, $\alpha = 2at_{so}$, and a is the lattice parameter. One should keep in mind

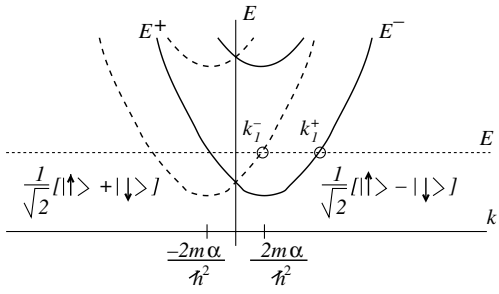

Fig. 2. Dispersion curve under spin–orbit coupling. For the stub transistor, the bias is set to select single mode transport.

that in the tight-binding approximation E_n - $E_n - 2t$ ($t_{so} = 0$).

In order to keep track of the eigenvalues, solve for $t_{so} = 0$ ($\alpha = 0$) to get E_n, then use the expression above to calculate the four values of the wavenumber for each eigenvalue. Use that to follow the eigenvalues and eigenvectors calculated with $t_{so} \neq 0$ ($\alpha \neq 0$).

The wavefunctions can be approximated by

$$\Psi_n^+(x,y) = \sum_n \phi_n(x) \frac{e^{ik_y y}}{\sqrt{2}} [|\uparrow\rangle + |\downarrow\rangle] \tag{12}$$

$$\Psi_n^-(x,y) = \sum_n \phi_n(x) \frac{e^{ik_y y}}{\sqrt{2}} [|\uparrow\rangle - |\downarrow\rangle] \tag{13}$$

As the carrier flows in the device with a given energy, it may have two different wavenumbers k_1^+ and k_1^-. Hence, there is a different phase, depending if the spin is up or down. The phase difference between paths is $2t_{so}/t$. The stub transistor can be used to select different type of carriers, and therefore could be used to built a spin filter. Considering $a = 0.25$ nm, $\alpha = 10^{-11}$ eV m, $m^* = 0.042m_0$, $2m\alpha a/\hbar^2 = 0.0656$, if $L = 1\ \mu m$, then $(\Delta k)a = 3.5\pi$, which is a quite large phase difference, which can be exploited in the stub transistor configuration. The difficulty with the single gate stub transistor is that the channel is closed at a very specific voltage, this shortcoming is reduced in the multiple gate configuration, as will be seen from the simulation results.

3. Simulation of electron transport

There are many approaches for the calculation of electron transport [34,37]. There is always a compromise between accuracy [28] and computing power [22]. For the purpose of this paper, we have chosen an approach which can be carried out with a personal computer [25].

Quantum effects are observed when one of the dimensions of the nanostructure is of the order of the Fermi wavelength. As the electron flows through the device, it may suffer scattering events. These events are classified as elastic or inelastic. In elastic scattering, the wavefunction preserves its phase coherence. In this work, it is assumed that all scattering events are coherent, i.e., the mean free path for inelastic scattering is larger than the device dimensions [25,32,33,35–37,39,40].

To calculate the current density, one can solve Schrödinger equation to obtain the wavefunctions, as presented in the previous section, then use the current operator shown in Eq. (14).

$$j_y = \frac{e\hbar}{2mi}[\Psi^\dagger \frac{\partial \Psi}{\partial y} - \frac{\partial \Psi^\dagger}{\partial y}\Psi] + \frac{e\alpha}{\hbar}\Psi^\dagger \sigma_x \Psi \tag{14}$$

In the quantum regime, Landauer [37] has shown that the conductance is related to the transmission probability, as given by Eq. (15).

$$G = g_v g_s G_Q \sum |T(E)|, \tag{15}$$

where $G_Q = e^2/h = 3.873 \times 10^{-5} S$ is the conductance quantum, and $g_s = 2$ is the spin degeneracy. $T(E)$ is the quantum transmission probability, $|T(E)| = 1$ for open channels, and $|T(E)| = 0$ for closed channels. As the energy, E, changes, channels will open or close. This step-like behavior of the conductance is observed experimentally. In a semiconductor, one has to include the valley degeneracy, g_v. The numerical value of g_v has a dependence on the cross-sectional shape [41].

To calculate the Landauer conductance, the quantum transmission probability must be obtained. This is achieved by calculating the electron wavefunctions. Various methods have been used for the calculation of the Landauer conductance in a nanodevice. Among such methods, one can mention the recursive Green function approach develop by MacKinnon [22], and used by Ando to study point contacts [23]. Nicolic and MacKinnon [24] have used this method to study the effect of the interface roughness on the electron transport. Another approach is the transfer function method, which was used by Gilbert and Ferry [27] in 3D simulation of the FD-SOI MOSFET. All examples presented above have used the tight-binding approximation for the Hamiltonian.

In this Hamiltonian, a set of wavefunctions, $\{\Psi_l\}$ ($l = l_1 l_2 l_3$), each localized at different site, form an orthonormal basis ($\int \Psi_l^* \Psi_m dr = \delta_{lm}$) for the solutions. The tight-binding Hamiltonian has a simple matrix representation (see Appendix A), hence it is quite suitable for numerical calculations.

A simplified assumption to reduce computational time, is that the wave functions associated with the lattice are localized with no superposition.

3.1. The algorithm

The device is divided into N slices. To setup the calculation, two extra slices are added, slice 0 and slice $N+1$, to represent the reservoirs. The confining potential, $V(x,y)$, is discretized in the square lattice, as shown in Fig. 3.

First, consider the device without spin–orbit coupling. Considering the matrix representation of the Hamiltonian, the tight-binding approximation results in a modified Schrödinger equation to include the interaction between neighbor sites, as shown in Eq. (16) [23]. To calculate the transmission probability, the wavefunction is calculated first at slice 0, by solving the eigenvalue problem using the $2M \times 2M$ system shown in the Appendix A (M is the number of sites per slice). The first line of the matrix is Schrödinger equation (Eq. (16)), and the second line is the condition $\Psi_i = e^{ika}\Psi_{i-1} = \lambda\Psi_{i-1}$, where a is the lattice parameter.

$$\left[\left(E + \lambda t + \frac{t}{\lambda}\right)\underline{I} - H_0\right]\Psi_i = 0 \tag{16}$$

Hence,

$$E_n = E + \lambda t + \frac{t}{\lambda} \tag{17}$$

For $E_n = E$, $\lambda = \pm i$, and $E_n - E = \pm 2t$, $\lambda = \pm 1$. The propagating modes with physical interest have $\lambda = 1$. Therefore, the conductance steps will occur at $E = E_n - 2t$. Making $E_n - E = 2t$ in Eq. (17), one gets an equation for λ.

$$\lambda^2 - 2\lambda + 1 = 0 \tag{18}$$

The spin–orbit coupling may be considered as a perturbation.

$$H = H_o + H_{so} \tag{19}$$

Using time-independent degenerate perturbation theory, one gets the following energy splitting due to the spin–orbit coupling

$$\Delta^{(1)} = \langle 0|H_{so}|0\rangle, \quad \Delta^{(2)} = \sum \frac{|\langle k|H_{so}|l\rangle|^2}{E_D^0 - E_{ki}^0}. \tag{20}$$

It is assumed that the perturbation is small, so that the second order term is negligible, therefore band mixing is neglected. This leads to

$$\alpha \ll \frac{\hbar^2}{mW} \tag{21}$$

$$t_{so} \ll \frac{t}{N} \tag{22}$$

To include the Rashba effect, one has to solve for the following eigenvalue problem [38]

$$\left[\left(E + \lambda t + \frac{t}{\lambda}\right)\underline{I} - H_0\right]\Psi_m^+ - \left[T_{so} + i\frac{t_{so}}{\lambda}\underline{I} - i\lambda t_{so}\underline{I}\right]\Psi_m^- = 0 \tag{23}$$

$$\left[\left(E + \lambda t + \frac{t}{\lambda}\right)\underline{I} - H_0\right]\Psi_m^- + \left[T_{so} - i\frac{t_{so}}{\lambda}\underline{I} + i\lambda t_{so}\underline{I}\right]\Psi_m^+ = 0 \tag{24}$$

where,

$$T_{so} = \begin{pmatrix} 0 & -t_{so} & 0 & \dots & 0 \\ t_{so} & 0 & -t_{so} & \dots & 0 \\ 0 & t_{so} & 0 & \dots & 0 \\ \vdots & \vdots & \vdots & & -t_{so} \\ 0 & 0 & 0 & \dots & 0 \end{pmatrix}. \tag{25}$$

If $t_{so} = 0$, Eq. (23) and (24) become degenerate and reduce to Eq. (16).

Substituting Ψ_m^+ of Eq. (24) into Eq. (23), one gets Eq. (26), which is a generalization to Eq. (16), to include spin–orbit coupling.

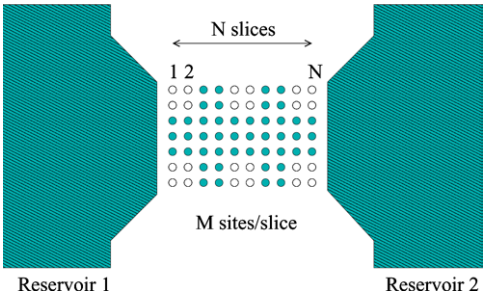

Fig. 3. Quantum device connecting two reservoirs. The device is divided in N slices, with M sites each, for a total of $N \times M$ sites.

$$(E\underline{I} - \underline{H}) \mp \mathrm{i}\underline{T}_{\mathrm{so}} + \lambda(t \mp t_{\mathrm{so}})\underline{I} + \frac{1}{\lambda}(t \pm t_{\mathrm{so}})\underline{I} = 0 \tag{26}$$

Notice that $\mathrm{i}\underline{T}_{\mathrm{so}}$ is hermitean.

$$E - E'_n + \lambda(t \mp t_{\mathrm{so}}) + \frac{1}{\lambda}(t \pm t_{\mathrm{so}}) = 0, \tag{27}$$

where E'_n is the solution of $H_0 \pm \mathrm{i}T_{\mathrm{so}} - E = 0$.

Solving for λ.

$$\lambda = \frac{E'_n - E \pm \sqrt{(E'_n - E)^2 - 4(t^2 - t_{\mathrm{so}}^2)}}{2(t \mp t_{\mathrm{so}})} \tag{28}$$

The matrix is now $4M \times 4M$.

sion of the program to simulate the quantum stub with applied voltages.

In our previous paper [42], we have simulate the one-sided stub transitor. In this work, we have simulated the double sided stub transitor. This configuration has the advantage of using a simetrical confining potential. As an example of the calculation, consider the configuration with one pair of stubs. The simulation is presented in Fig. 4. The confining potential has a barrier of $2E_{\mathrm{F}}$, the width of the main wire is $W = 10$ nm, the grid parameter is $a = 0.5$ nm, and the length of main wire is $L = 275$ nm. The stubs are 48 nm long on each side of the wire.

$$\begin{pmatrix} t^{-1}(\underline{H}_{i,i} - E\underline{I}) & -\underline{I} & t^{-1}\underline{T}_{\mathrm{so}} & \mathrm{i}t^{-1}t_{\mathrm{so}} \\ \underline{I} & \underline{0} & \underline{0} & \underline{0} \\ -t^{-1}\underline{T}_{\mathrm{so}} & \mathrm{i}t^{-1}t_{so} & t^{-1}(\underline{H}_{i,i} - E\underline{I}) & -\underline{I} \\ \underline{0} & \underline{0} & \underline{I} & \underline{0} \end{pmatrix} \begin{pmatrix} \underline{\Psi}_i^+ \\ \underline{\Psi}_{i-1}^+ \\ \underline{\Psi}_i^- \\ \underline{\Psi}_{i-1}^- \end{pmatrix} = \lambda \begin{pmatrix} \underline{I} & \underline{0} & \mathrm{i}t^{-1}t_{\mathrm{so}}\underline{I} & 0 \\ \underline{0} & \underline{I} & \underline{0} & \underline{0} \\ \mathrm{i}t^{-1}t_{\mathrm{so}}\underline{I} & \underline{0} & \underline{I} & \underline{0} \\ \underline{0} & \underline{0} & \underline{0} & \underline{I} \end{pmatrix} \begin{pmatrix} \underline{\Psi}_i^+ \\ \underline{\Psi}_{i-1}^+ \\ \underline{\Psi}_i^- \\ \underline{\Psi}_{i-1}^- \end{pmatrix} \tag{29}$$

The transmission probability is related to the Green function.

$$T(E)_{ij} = -t[\underline{U}^{-1}(+)\underline{G}(E)_{N+1,0}(\Lambda(-) - \Lambda(+))\underline{U}(+)]_{ij} \tag{30}$$

Now the conductance can be calculated under the Landauer formalism as a sum of the two spin components.

$$G = G^{\mathrm{up}} + G^{\mathrm{down}} = g_{\mathrm{v}}\frac{\mathrm{e}^2}{h}\left[\sum_u |T_{\mathrm{u}}^{\mathrm{up}}|^2 + \sum_{\mathrm{v}} |T_{\mathrm{v}}^{\mathrm{down}}|^2\right] \tag{31}$$

We have implemented this algorithm in C using CLAPACK, and now the program is being extended to include the application of a voltage potential to the stubs.

4. Results and discussion

The stubbed waveguide consists of a nanowire with one or more periodically spaced stubs [42]. Here, we present the results without spin–orbit coupling as we are extending the spin–orbit ver-

In Fig. 5, the simulation results for the double-stub configuration is presented. The parameters are all the same as in the single pair case. Except that, now there two pais space 10 nm from each other. Notice that for the double stub, one gets a

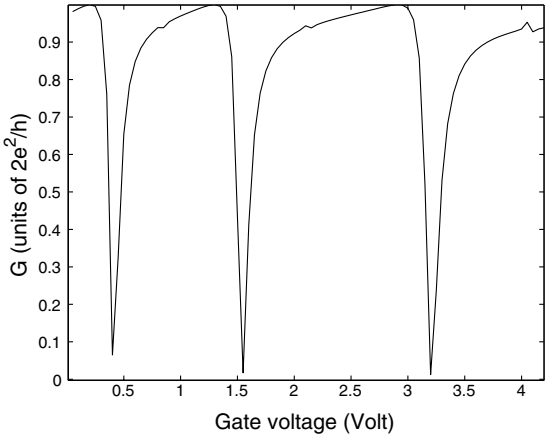

Fig. 4. Simulation of the quantum transistor with one pair of symmetrical stubs. The voltage barrier is $2E_{\mathrm{F}}$, $W = 10$ nm, $a = 0.5$ nm, and $L = 275$ nm (length of main wire). Stub length is 48 nm.

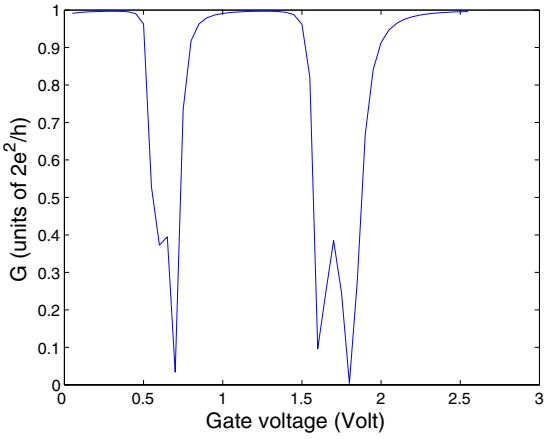

Fig. 5. Simulation of a double gate quantum stub transistor. The presence of the double gate generate a doublet. The voltage barrier is $2E_F$, $W = 10$ nm, $a = 0.5$ nm, and $L = 275$ nm (length of main wire). Stub length is 48 nm, and spaced 10 nm.

dublet at each anti-resonance. The consequence is that the transmission zero has now become a blocked region, and not only a single voltage zero, as for the single stub.

With three stubs one has a triplet (Fig. 6). The blocked region is even wider. For this simulation the stub pairs are spaced of 10 nm. The other parameters are identical to the previous simulations. Each simulation takes over 10 h on pentium IV class microcomputer.

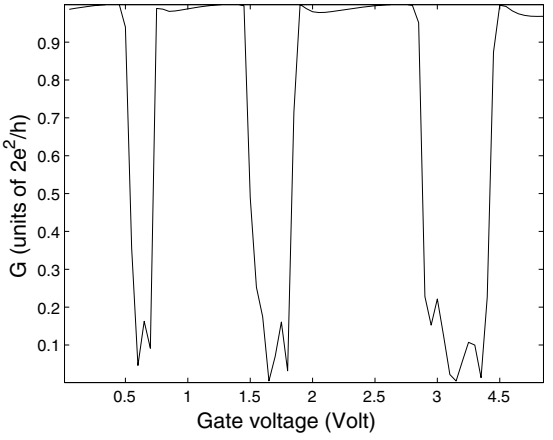

Fig. 6. In the triple gate configuration the block region is much wider. The voltage barrier is $2E_F$, $W = 10$ nm, $a = 0.5$ nm, and $L = 275$ nm (length of main wire). Stub length is 48 nm, and spaced 10 nm.

5. Conclusions

The numerical simulation of the DC transport of the multiple gate stub transistor has been presented. We have also shown how the spin–orbit coupling can be introduced into the program. The program is based on the recursive Green function technique to calculate the quantum transmission probability. This approach has the advantage of making it easier to simulate different device geometries.

The simulation results show that the multiple gate stub transistor displays a much wider antiresonance region. This is a positive step in making such devices practical.

We have rewritten the program to include spin–orbit coupling, and our next step is to introduce the possibility of applying an external voltage to the stubs, which will be presented in our next paper.

Acknowledgement

This work has been supported by CNPq (Brazilian agency) through the *Instituto do Milênio* innitiative.

Appendix A

The Schrödinger equation of the device is written as shown in Eq. (A.1). The diagonal matrices, $\underline{H}_{ii}$ $(i = 1, \ldots N)$, represent the slices and the off-diagonal matrices represent the coupling between neibhoring layers.

$$\begin{pmatrix} \underline{H}_{11} & \underline{V}_{12} & 0 & \ldots & 0 \\ \underline{V}_{21} & \underline{H}_{22} & \underline{V}_{23} & \ldots & 0 \\ 0 & \underline{V}_{32} & \underline{H}_{33} & \ldots & 0 \\ \vdots & \vdots & \vdots & & \vdots \\ 0 & 0 & 0 & \ldots & \underline{H}_{NN} \end{pmatrix} \begin{pmatrix} \underline{\Psi}_1 \\ \underline{\Psi}_2 \\ \underline{\Psi}_3 \\ \vdots \\ \underline{\Psi}_N \end{pmatrix} = E \begin{pmatrix} \underline{\Psi}_1 \\ \underline{\Psi}_2 \\ \underline{\Psi}_3 \\ \vdots \\ \underline{\Psi}_N \end{pmatrix}, \tag{A.1}$$

where $\underline{V}_{ii+1} = -\frac{\hbar^2}{2m^*a^2}\underline{I} = -t\underline{I}$

This equation can be solved using the Green function technique.

$$(E\underline{I} - \underline{H})\underline{G} = \underline{I}, \tag{A.2}$$

where $\underline{I}$ is the identity matrix, and $\underline{G}$ is the Green function matrix.

The solution of this eigenvalue problem yields two sets of eigenfunctions and eigenvalues. One set propagates to the left, and the other to the right. The eigenfunction can be combined in a matrix. The left-going waves is represented as $\underline{U}(-)$ and the right-going waves is represented as $\underline{U}(+)$. To decide the direction of propagation, one checks the eigenvalues associated with the eigenfunction. If the eigenvalue is real and less then one, it is a right-going evanescent mode, a real eigenvalue larger then one is a left-going evanescent mode. For complex eigenvalue, one should check the imaginary part. If the imaginary part of the eigenvalue is positive the wavefunction is propagating to the right. A negative imaginary part is a wavefunction propagating to the left. Equivalently, one can combine the eigenvalues in a diagonal matrix form, $\underline{\Lambda}(-)$ for the left-going waves and $\underline{\Lambda}(+)$ for the right-going waves. These wavefunctions are used to calculate the initial Green function $\underline{G}_{00}$,

$$\underline{G}_{00} = [E\underline{I} - \underline{H}_0 - t(U(-)\Lambda(-)^{-1}U(-)^{-1})]^{-1}. \tag{A.3}$$

To include scattering, consider that at the 0th slice, the wavefunction has two components, one incident and the other reflected ($\Psi_0 = \Psi_0^{(+)} + \Psi_0^{(-)}$). At the $N+1$-slice there is only the transmitted component ($\Psi_{N+1} = \Psi_{N+1}^{(+)}$).

$$\begin{pmatrix} \underline{\Psi}_0 \\ \underline{\Psi}_1 \\ \vdots \\ \underline{\Psi}_{N+1} \end{pmatrix} = \begin{pmatrix} \underline{G}_{00} & \underline{G}_{01} & \cdots & \underline{G}_{0,N+1} \\ \underline{G}_{10} & \underline{G}_{11} & \cdots & \underline{G}_{0,N} \\ \vdots & \vdots & \vdots & \vdots \\ \underline{G}_{N+1,0} & \underline{G}_{N+1,1} & \cdots & \underline{G}_{N+1,N+1} \end{pmatrix} \begin{pmatrix} \underline{V}_0 \\ 0 \\ \vdots \\ 0 \end{pmatrix} \tag{A.4}$$

The Green function can be thought as making the connection between the two reservoirs. Its calculation can be used to get the transmission probability.

$$\underline{\Psi}_{N+1}^{(+)} = \underline{G}_{N+1,0}\underline{V}_0 \tag{A.5}$$

The Hamiltonian matrix of a slice is constructed with $H_{ii} = V(\text{slice}, i) - 4t$ (two dimensional), and $H_{i,i+1} = H_{i+1,i} = -t$, where t is the coupling strength between sites. The Hamiltonian matrix, $\underline{H}$, is $M \times M$.

$$\underline{H}_i = \begin{pmatrix} V_1 - 4t & -t & 0 & \cdots & 0 \\ -t & V_2 - 4t & -t & \cdots & 0 \\ 0 & -t & V_3 - 4t & \cdots & 0 \\ \vdots & \vdots & \vdots & & \vdots \\ 0 & 0 & 0 & \cdots & V_M - 4t \end{pmatrix} \tag{A.6}$$

where V_i in the diagonal is the confining potential energy profile at a given slice. This potential energy is the device profile.

The calculation starts with $\underline{G}_{00}$ and the device is constructed recursively slice by slice until the $N+1$ slice is reached. As the slices are added, the new value of the Green function is calculated as follows:

$$\underline{G}_{i+1,i+1} = [E\underline{I} - \underline{H}_i - t^2\underline{G}_{i,i}]^{-1}$$

$$\underline{G}_{i+1,0} = -t\underline{G}_{i+1,i+1}\underline{G}_{i,0} \tag{A.7}$$

Finally, at the second reservoir

$$\underline{G}_{N+1,N+1} = [E\underline{I} - \underline{H}_N - t\underline{U}(+)\underline{\Lambda}(+)\underline{U}^{-1}(+) - t^2\underline{G}_{N,N}]^{-1}$$

$$\underline{G}_{N+1,0} = -t\underline{G}_{N+1,N+1}\underline{G}_{N,0} \tag{A.8}$$

References

[1] A.B. Guerra, E.J.P. Santos, in: Proceedings of the XVIII International Symposium on Devices and Technology, Electrochemical Society Proceedings, PV2003-09, New Jersey, 2003, pp. 197–204.
[2] E. Polizzi, N. Ben Abdallah, Phys. Rev. 66 (2002) 245301.
[3] P. Debray, O.E. Raichev, P. Vasilopoulos, M. Rahman, R. Perrin, W.C. Mitchell, Phys. Rev. B 61 (2000) 10950.
[4] J. Appenzeller, Ch. Schroer, J. Appl. Phys. 87 (2000) 3165.
[5] P. Debray, O.E. Raichev, M. Rahman, R. Akis, W.C. Mitchel, Appl. Phys. Lett. 74 (1999) 768.
[6] K. Nikolić, R. Šordan, Phys. Rev. B 58 (1998) 9631.
[7] M. Khatun, P.K. Joyner, R.M. Cosby, Y.S. Joe, J. Appl. Phys. 84 (1998) 3409.
[8] C.A. Flory, J. Appl. Phys. 82 (1997) 6306.
[9] R. Akis, P. Vasilopoulos, P. Debray, Phys. Rev. B 56 (1997) 9594.

[10] J. Appenzeller, Ch. Schroer, Th. Schäpers, A.v.d. Hart, A. Förster, B. Lengeler, H. Lüth, Phys. Rev. B 53 (1996) 9959.
[11] R. Šordan, K. Nikolić, Phys. Rev. B 52 (1995) 9007.
[12] K. Aihara, M. Yamamoto, T. Mizutani, Appl. Phys. Lett. 63 (1993) 3595.
[13] Y. Takagaki, D.K. Ferry, Phys. Rev. B 45 (1992) 6715.
[14] F. Sols, M. Macucci, U. Ravaioli, K. Hess, J. Appl. Phys. 66 (1989) 3892.
[15] (a) S. Datta, B. Das, Appl. Phys. Lett. 56 (1989) 665;
(b) Igor Žutić, Jaroslav Fabian, S. Das Sarma, Rev. Mod. Phys. 76 (2004) 323.
[16] R. Winkler, Phys. Rev. B 62 (2000) 4245–4248.
[17] J. Nitta, T. Akazaki, H. Takayanagi, T. Enoki, Phys. Rev. Lett. 78 (1997) 1335.
[18] J.P. Heida, B.J. van Wees, J.J. Kuipers, T.M. Klapwijk, G. Borghs, Phys. Rev. B 57 (1998) 11911.
[19] T. Ando, H. Tamura, Phys. Rev. B 46 (1992) 2332–2338.
[20] A.V. Moroz, C.H.W. Barnes, Phys. Rev. B 60 (1999) 14272–14285.
[21] X.F. Wang, P. Vasilopoulos, Phys. Rev. B 68 (2003) 035305.
[22] A. MacKinnon, Z. Phys. B 59 (1985) 385.
[23] T. Ando, Phys. Rev. B 44 (1991) 8017–8027.
[24] K. Nikolić, A. MacKinnon, Phys. Rev. B 50 (1994) 11008–11017.
[25] E.J.P. Santos, in: Proceedings of the XVII International Symposium on Devices and Technology, Electrochemical Society Proceedings, 2002-8, Pennington, NJ, 2002, pp. 56-64.
[26] G. Feve, W.D. Oliver, M. Aranzana, Y. Yamamoto, Phys. Rev. B 66 (2002) 155328.
[27] M.J. Gilbert, D.K. Ferry, J. Appl. Phys. 95 (2004) 7954–7960.
[28] P.S. Krstić, X.-G. Zhang, W.H. Butler, Phys. Rev. B 66 (2002) 205319.
[29] (a) James D. Bjorken, Sidney D. Drell, Relativistic Quantum Mechanics, McGraw-Hill, New York, 1964, p. 46;
(b) L.L. Foldy, S.A. Wouthuysen, Phys. Rev. 78 (1950) 29.
[30] Alexander J. Silenko, J. Math. Phys. 44 (2003) 2952–2966.
[31] M. Governale and U. Zuelicke, cond-mat/0407036, 2004.
[32] Rolf Landauer, Physica A 168 (1990) 75.
[33] David K. Ferry, Robert O. Grondin, Physics of Submicron Devices, Plenum Press, New York, 1991.
[34] Richard L. Liboff, Kinetic Theory: Classical, Quantum, and Relativistic Descriptions, Prentice-Hall Advanced Reference Series, New Jersey, 1990, p. 130.
[35] H. Baranger, A. Douglas Stone, Phys. Rev. B 40 (1989) 8169.
[36] A.D. Stone, Physics of nanostructures, in: J.H. Davies, A.R. Long (Eds.), Proceedings of the 38th Scotish Universities Summer School in Physics, Institute of Physics, Bristol, 1992, p. 65.
[37] (a) Rolf Landauer, IBM J. Res. Dev. 1 (1957) 223;
(b) Rolf Landauer, Philos. Mag. 21 (1970) 863.
[38] F. Mireles, G. Kirczenow, Phys. Rev. B 64 (2001) 024426.
[39] F.A. Buot, Phys. Rep. 234 (1993) 73–174.
[40] D.K. Ferry, C. Jacoboni (Eds.), Quantum Transport in Semiconductors, Plenum Press, New York, 1992.
[41] Y. Nakajima, Y. Takahashi, S. Horiguchi, K. Iwadate, H. Namatsu, K. Kurihara, M. Tabe, Jpn. J. Appl. Phys. 34 (1995) 1309–1314.
[42] A.B. Guerra, E.J.P. Santos, J. Int. Cir. Sys. 1 (2004) 36–40.